Exp Fluids (2008) 45:633–642
DOI 10.1007/s00348-008-0520-6

RESEARCH ARTICLE

Image analysis applied to the study of mixing in a stably stratified shear layer

Giorgio Querzoli · Paolo Monti · Antonio Cenedese

Received: 15 November 2007 / Revised: 19 March 2008 / Accepted: 17 May 2008 / Published online: 14 June 2008

Abstract The development and breaking of Kelvin–Helmholtz waves is one of the primary causes of mixing in many geophysical and engineering flows with layers of fluids having different densities and horizontal velocities. Although this phenomenon was extensively studied in the field, a complete description can be experimentally obtained only by the use of image analysis techniques that are applicable only in laboratory experiments. The particular nature of the flow, especially before the development of the waves when the flow is parallel but in opposite direction, makes the application of the classical image velocimetry techniques non-trivial. With this in mind, a stably stratified shear flow was reproduced in the laboratory by means of a tilting tank. The velocity and density fields were measured simultaneously with multipoint time-resolved techniques during the formation and development of the Kelvin–Helmholtz waves. A novel particle tracking procedure is proposed that includes the stretching of the acquired images in the direction orthogonal to the main motion. Tests on synthetic images show a meaningful improvement in the effectiveness of particle tracking when using the proposed technique. Laser-Induced Fluorescence (LIF) data have been acquired by a second camera, equipped with a band-pass filter in order to measure only the fluoresced light. Particle Tracking Velocimetry (PTV) and LIF data have been referenced to the same frame by a registration procedure based on an affine transformation. In the range of the parameters investigated during the experiments, the evolution of the interface thickness and sharpness scales with the advective time scale. The analysis of the space–time evolution of the longitudinal statistics gives a comprehensive picture of the development and breaking of the waves.

G. Querzoli (✉)
Dipartimento di Ingegneria del Territorio,
Università degli studi di Cagliari, Via Marengo 3,
09123 Cagliari, Italy
e-mail: querzoli@unica.it

P. Monti · A. Cenedese
Dipartimento di Idraulica Trasporti e Strade,
Università di Roma "La Sapienza", Roma, Italy

1 Introduction

The study of mixing across stably stratified layers of fluids is of interest in a wide range of geophysical flows including the atmosphere and oceans, and in engineering applications like flows in combustion chambers and chemical reactors. The destabilisation induced by a velocity gradient, with the subsequent generation and development of Kelvin–Helmholtz (KH) waves, is one of the most significant causes of mixing, despite the stabilising action of a stratification (Peltier and Caulfield 2003). In field experiments, velocity and density data (or any other scalar) are routinely collected by point measurements or, in the best case, by profiler soundings (Woods 1968; De Silva et al. 1996; Monti et al. 2002). Although these investigations permit a quantification of the mean fluxes involved in the mixing process, they cannot give a full picture of the phenomenon since they describe the spatial variation of the measured quantities at most along one direction. Recently, this limitation motivated a number of numerical studies with the aim of capturing the detailed mechanisms involved in the generation and breaking of the KH waves (Smyth and Moum 2000; Caulfield and Peltier 2000; Staquet 2000). The only way to experimentally obtain a comparable amount of information is to reproduce the phenomenon in

the laboratory, since developments in image analysis allow the use of measurement techniques that yield a full two-dimensional description of the phenomenon in the investigation plane. Among others, Troy and Koseff (2005) investigated breaking internal waves using the LIF technique, while Monti et al. (2007) analysed in detail some mixing properties of stably stratified shear layers by using quantitative observational data taken from the same experimental facility described herein.

The KH waves have been generated in a tilting tank following the pioneering idea of Thorpe (1968), and described in detail in Defina et al. (1999). The density of the fluid was measured indirectly by means of LIF, and the velocity by PTV, using two video-cameras simultaneously. Finally, the two data sets have been referenced to the same reference frame.

LIF has been frequently used to obtain snapshots of the spatial variability of the density field in stratified flows, but application of image velocimetry to the flow considered here is more difficult because of its peculiar characteristics. During the initial stage, in fact, the flow is dominated by two counter-flowing layers separated by a sharp, sheared density interface. As a consequence, both high velocities and an intense velocity gradient are present. The flow is strongly anisotropic with large longitudinal velocities and small velocities in the transverse direction (as the flow is initially laminar). Conversely, during the development and breaking of the KH waves, the flow has a more complex structure, characterised by longitudinal velocities that are much smaller than during the previous stage. Moreover, one dimension of the measuring area coincides with the height of the tank, while the second dimension should be about two wavelengths in order to comprehensively describe the phenomenon. Therefore, the resulting region of interest on the digital images is very elongated, with a small resolution in the transverse direction (for example, in the present measurements the width of the images was 1 K pixels, while their height was only 256 pixels). Particle Image Velocimetry (PIV) is not suitable in that case, since it does not derive the velocity point-wise, but from interrogation regions whose transverse dimension would be comparable with the size of the tank height. This is particularly true during the first steps of the calculation, when larger windows are chosen in order to be able to measure the high longitudinal velocities. Conversely, PTV extracts the velocity from the displacement of a single particle, and therefore gives measurements at nearly a single point. On the other hand, PTV, which is generally much less robust than PIV, requires that the larger the velocities the lower the particle density, in order to be able to successfully recognise trajectories. However, if there are not enough particles, the structure of the velocity field cannot be deduced comprehensively.

With this in mind, a technique based on image deformation is proposed here in order to successfully track a larger number of particles, also during the first phase of the phenomenon when higher velocities are measured. The method is applicable to other parallel flows, including those with high velocity gradients. The paper is organized as follows: a description of the experimental procedure is given in Sect. 2; Sect. 3 deals with the details of the image analysis method, while Sect. 4 presents quantitative measurements pertinent to the KH waves.

2 Experimental set-up and procedures

The KH waves were generated in a Plexiglas tilting tank, 3700-mm long, 240-mm wide and 22-mm deep (Fig. 1). The tank was initially oriented vertically and filled halfway with an aqueous ethanol solution. Then, the remaining volume was carefully filled from below with a denser water–salt mixture. A peristaltic pump was used to fill the tank in order to not heat the fluid. A compliance and a head loss were added in the circuit connecting the pump with the tank in order to smooth the pulsatility of the flow generated by the pump. In addition, the flow rate during the filling process was very slow to avoid mixing between the two fluids. The solutions for the two layers were prepared in order to have the required density difference and identical refraction index (McDougall 1979). A refractometer with an accuracy of $\pm 10^{-4}$ was used to verify this. This method enables the exploration of the general characteristics of the KH instabilities via quantitative density measurements through the LIF technique (Atsavapranee and Gharib 1997; Troy and Koseff 2005, among others). Pine pollen particles, 20 μm in diameter, were dispersed in both the solutions to be used as PTV tracers. The upper layer was premixed with a fluorescent dye (Sodium fluorescein) for the LIF measurements. Mixing of aqueous ethanol and salt solutions having the same refractive index generates a new mixture with an index of refraction slightly different from that of the original solutions. This variation, however, was very small during the experiments and did not produce any significant visual distortions. Next, the tank was rotated

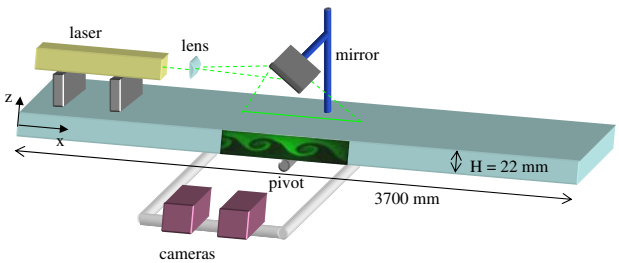

Fig. 1 Sketch of the experimental set-up

carefully up to the horizontal. Two fluid layers of equal depth ($H/2 = 11$ mm) and different densities, separated by a sharp interface, were generated. After about 30 min all motions due to the filling procedure subsided and the tilting of the tank from its horizontal position to a known angle, θ, provided the acceleration in opposite directions of the two layers (Fig. 2a). The ascending, upper-layer fluid and the descending, lower-layer fluid, generated shear at the interface which led to the formation of a series of KH waves (Fig. 2b) followed by their collapse and associated intense vertical mixing (Fig. 2c). The waves were stationary with respect to the tank since the depth of the two fluids was the same, so that the opposing velocities in the two layers were of the same magnitude. As a consequence, the billows remained in the area framed by the cameras during their whole life cycle.

3 Image analysis methods

The investigation area was rectangular (100 mm × 22 mm), lying in the vertical, middle plane of the tank, and parallel to its longest axis. It was illuminated with a thin (1.5 mm), Argon-ion laser sheet. The area was large enough to include more than one KH wave, from their formation to the collapse. The laser was used in all-lines mode with a power of about 300 mW. The aqueous ethanol solution, dyed with fluorescein, has a peak of absorption at about 514 nm and a peak of emission at about 540 nm. Images were captured by two cameras fixed to the tank, both framing the illuminated area.

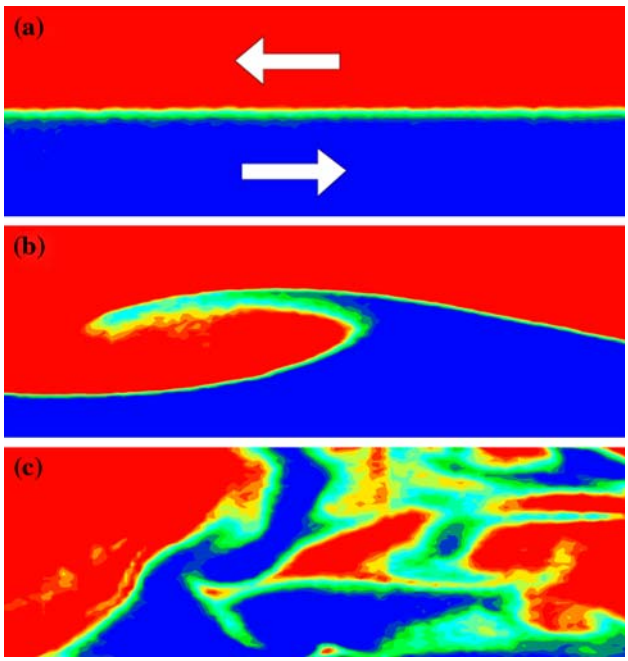

Fig. 2 Example of image sequence taken during (**a**) the phase of parallel shear flow, (**b**) the KH wave formation, and (**c**) the wave collapse. In (**a**) the *arrows* indicate the flow direction. *Red* and *blue* indicate regions of bright (light) and dark (heavy) fluid, respectively

3.1 Density measurements

The light emitted by the fluorescein was captured by a digital CCD camera at 25 frames per second equipped with a filter tuned to 540 nm to allow only the fluorescence and not the laser light to pass. Exposure time was 10^{-2} s. The resolution of the camera was 512 × 720 pixels × 8 bit. The distribution of the light intensity in the framed area was measured by acquiring a reference image with a uniformly low concentration of fluorescein. The dye concentration at a given pixel, which, in turn, was directly proportional to the fractional volume of the dyed fluid, was assumed proportional to the luminosity measured during the experiment, normalised by the reference image at the same location. The variation of the luminosity, on the reference images, along the laser light path gives an estimate of the effect of the light adsorption on the measurement. During the present experiments, it was observed to be always negligible. Note that the use of the fluorescein as the marker for the density is reasonable since fluorescein ($Sc \cong 1000$) and salt ($Sc \cong 700$) have similar Schmidt number, $Sc = \nu/\kappa_\rho$ (where ν and κ_ρ are the kinematic viscosity and the molecular diffusivity of mass, respectively). The spatial resolution of the images (about 86 μm/pixel) is limited by the need to frame horizontally more than one Kelvin–Helmholtz wavelength with the camera. Therefore, the resolution could be not high enough to measure the smaller scales of mixing during some short time intervals, such as immediately after the wave break. However, the salient aspects of the phenomenon are well described before and after those short periods.

3.2 Velocity measurements

As mentioned above, PTV was chosen for the velocity measurement because it extracts velocity samples from individual particles, therefore with a higher spatial resolution than PIV, which is based on the correlation of interrogation windows. Moreover, PTV also works effectively with a lower number of tracer particles. This is a benefit because particles may perturb the colour and the intensity of the fluoresced light, thus affecting the quality of the LIF measurements. PTV images were acquired by means of a high-speed, CMOS camera, 1024 × 256 × 8 bit in resolution, with a frame rate of 250 Hz. The particles were identified by thresholding the images after a dynamical background subtraction. For each image, the background

was computed as the moving average over an area four or five times larger than particles. Subtraction of the background has two positive effects: it corrects for non-uniformity of illumination on the analysed area and it enhances the contrast in the neighbourhood of the particles, thus significantly improving the particle recognition.

Trajectories were reconstructed by connecting particles of successive frames according to the following criteria: (i) initial particle velocity cannot exceed a given value, u_{max}; (ii) particle acceleration must be less than an assigned value, a_{max}; (iii) it is better to continue an existing trajectory rather than create a new one (the structure of the tracking algorithm is described in detail in Querzoli 1996). Velocity and acceleration thresholds have to be tuned as low as possible, but high enough to not cut-off any realistic displacement of the particles. However, such a general algorithm cannot work successfully with a flow such as the one under investigation. It must be noted that the above thresholds u_{max} and a_{max} are isotropic (i.e. act in the same way in the longitudinal and transverse displacements), but the flow, especially in its initial stage of development, is not, since it is a parallel flow with high longitudinal and very small transverse velocity. Moreover, PTV requires the mean distance between frames to be less than the distance covered by a particle between two frames. During the initial stage of the flow, particles covered a distance that was a meaningful fraction of the vertical depth H of the tank. Therefore, searching successfully for the next position of a particle would require examination of a wide portion of the investigation area, including the whole depth of the flow. However, imposing a low seeding level would result in a poorly detailed description of the flow. Furthermore, the low seeding level would be a disadvantage during the successive development and breaking of the KH waves, even if in that phase the typical velocities are much lower.

Here we propose a method to enhance PTV performance for the investigation of parallel shear flows with high velocity in the longitudinal direction and high transverse gradients. It consists of the stretching of the frames along the transverse dimension of a factor k_s before performing the particle and trajectory recognition procedures described above. Analysing the stretched images gives the following beneficial effects:

- increase in the mean distance between particles, $r = \sqrt{\frac{N_r \cdot N_c}{N_p}}$ (where N_r indicates the number of rows of the images, N_c the number of columns and N_p the number of particles on the image), allowing a higher seeding level to be used, or reducing ambiguities during the trajectory recognition;
- increase in the resolution of the vertical velocity measurements (this is particularly meaningful because the transverse velocities are small);
- isotropisation of the apparent particle motion, with an increase in the vertical displacements, compared to the horizontal ones. This makes the isotropic criteria based on the parameters u_{max} and a_{max} more suitable for the flow analysis.

The optimal value of the parameter k_s was found to be 3 for the current experiment. In order to check the effectiveness of the pre-stretching of the images, some preliminary tests were performed using synthetic images reproducing the salient characteristics of the initial, parallel sheared flow. A longitudinally uniform profile of the mean velocity, with two counter-flowing layers, was chosen (Fig. 3):

$$u = u_0 \tanh\left(4 \cdot \pi \cdot \left(\frac{z}{H} - 1\right)\right).$$

Particle trajectories have been simulated adding to the mean motion time-correlated perturbations generated by means of the Langevin equation (Monti and Leuzzi 1996), with an assigned, uniform standard deviation, σ, in both directions, and a Lagrangian, integral time-scale as long as 20 frames. Particle images had a Gaussian luminosity distribution with a standard deviation of 3.0 ± 1.5 pixels. Each data set consisted of 1000 consecutive frames $1024 \times 256 \times 8$ bits in resolution.

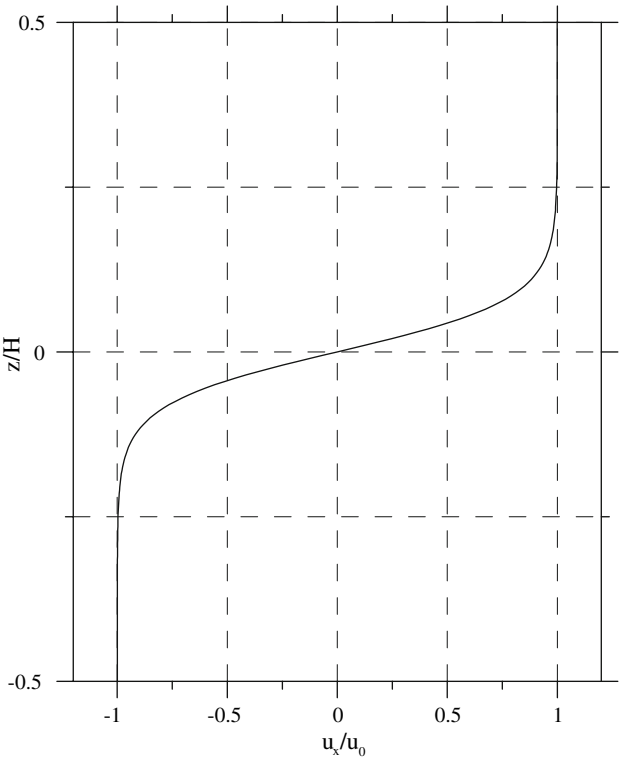

Fig. 3 Vertical profile of longitudinal velocity used to generate the synthetic images

Two "turbulence" intensities have been considered: a low turbulence case with $\sigma/u_0 = 0.02$, and a high turbulence case with $\sigma/u_0 = 0.10$, whereas the maximum velocity $u_0 = 20$ pixel/frame was kept the same during all the tests. For each turbulence level, a set of image series was generated changing the particle number in order to let the mean particle distance, r, range between $2d_0$ and $10d_0$ (where d_0 is the maximum displacement of the particles between frames, which, in turn, corresponds numerically to u_0 as far as velocities are measured in pixel/frame). Then images were analysed by the PTV algorithm both applying the frame stretching and without any pre-processing. The standard deviations of the longitudinal (σ_x) and transverse (σ_z) velocity component were computed on the whole measurement area, by subtracting the local mean velocity from each velocity sample.

Figure 4 shows the measured standard deviations as a function of the mean particle distance r normalised by the maximum particle displacement between frames, d_0, in the low turbulence case. A blue, horizontal line indicates the assigned level, $\sigma = 0.02u_0$. For large mean relative particle distances the ambiguity in the trajectory recognition is uncommon, so the measured standard deviation tends to the assigned value both with and without stretching. Furthermore, the standard deviation of the longitudinal component of the measured values is always a little higher than the assigned one (Fig. 4a). As the number of particles increases, and the relative distance decreases, the difference between the analysis of stretched and non-stretched images becomes more meaningful. In particular, appreciable deviations of σ/u_0 from the assigned value are observable at $r/d_0 \cong 6$ analysing the original images, whereas the relative distance can be reduced down to about 4 before the increase in the standard deviation becomes apparent when analysing the stretched images. The standard deviation of the transverse component maintains a good agreement with the assigned values down to a fractional mean particle distance $r/d_0 = 2$ (Fig. 4b).

The same overall behaviour is observed for the high turbulence level (Fig. 5). In this case, the analysis of the stretched images does not yield any meaningful variation from the assigned standard deviation for the transverse velocity component (Fig. 5b); conversely, without pre-processing, meaningful errors begin to appear for relative distances lower than 6. As for the low turbulence case, a

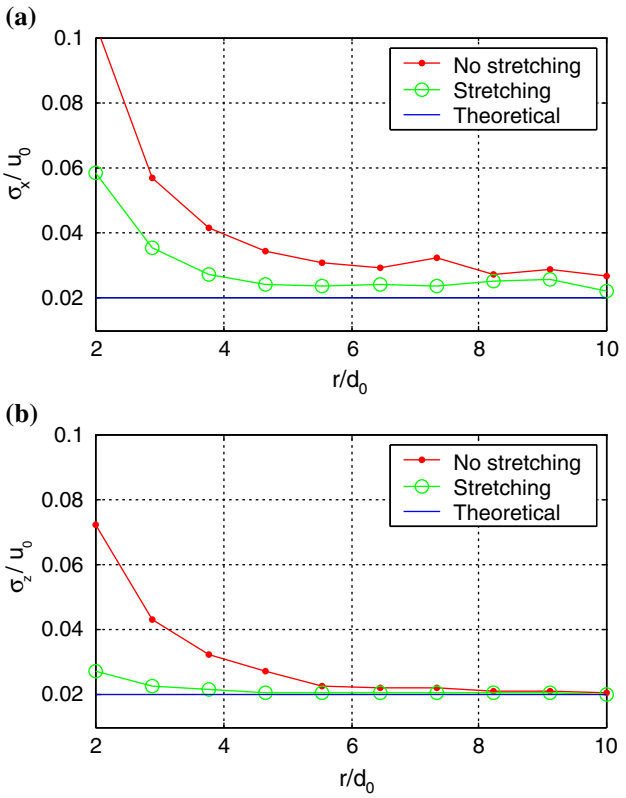

Fig. 4 Standard deviation of (**a**) the longitudinal and (**b**) transverse (*lower plot*) velocity measured by PTV as a function of the mean particle distance for the low turbulence case. Results obtained without stretching are plotted in *red*; results obtained with stretching are plotted in *green*. The *blue line* indicates the theoretical standard deviation

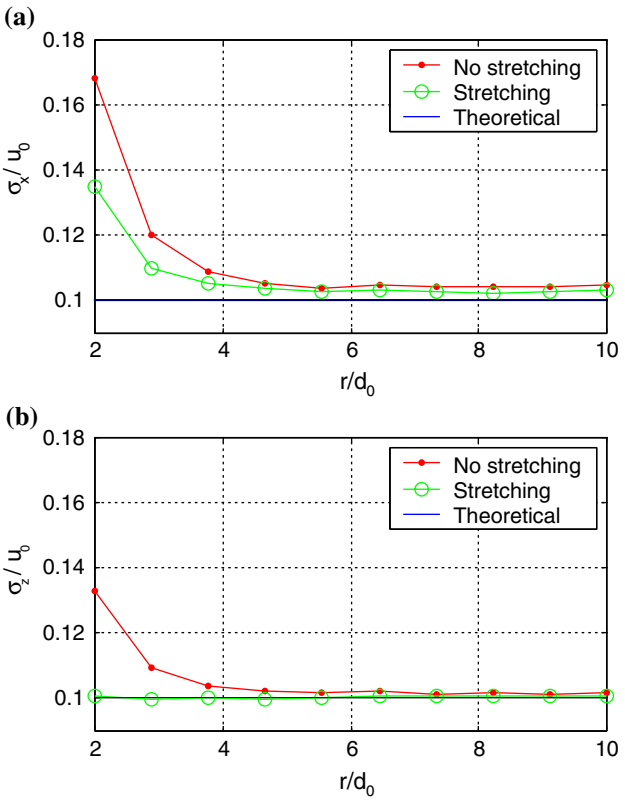

Fig. 5 Standard deviation of the (**a**) longitudinal and (**b**) transverse velocity measured by PTV as a function of the mean particle distance for high turbulence case. Results obtained without stretching are plotted in *red*; results obtained with stretching are plotted in *green*. The *blue line* indicates the theoretical standard deviation

small bias in the standard deviation of the longitudinal component appears irrespective of the relative distance (Fig. 5a). Without stretching the standard deviation begins to increase significantly for r lower than $5d_0$, whereas using the stretching this limit value is lowered down to about $4d_0$.

In summary, the analysis of stretched images gives better results whatever the relative distance. The improvement in using the stretching is larger in the transverse direction, and increases significantly as the relative distance between the particle decreases. These results may be affected by experimental conditions and PTV algorithm, but the general trend should also be valid in different conditions, given that the above results are obtained from synthetic images and the PTV algorithm is basic and general purpose.

3.3 Image registration

The fluid density information given by the LIF camera was spatially related to the velocity fields obtained from the high-speed camera by a registration procedure which did not require any calibration targets to be placed in the vessel (Zitová and Flusser 2003). Two simultaneous images of particles, dispersed within the fluid at rest, were acquired by the two cameras. Particle positions were computed from the two images. The affine transformation,

$$\vec{x}'' = A\vec{x}' + \vec{b},$$

that best mapped the positions, $\vec{x}'$ of the particles viewed from the filtered camera on the positions, $\vec{x}''$, recognised by the high-speed camera was found by minimizing the mean square error:

$$\varepsilon = \frac{1}{N}\sum_{k=1}^{N}\left[\vec{x}''_k - \left(A\vec{x}'_k + \vec{b}\right)\right]^2,$$

where $\vec{x}'_k$ and $\vec{x}''_k$ indicate the position of the kth particle on the LIF and PTV camera, respectively, and N indicates the number of particles on the images. The optimal affine transformation was used to map the density field onto the velocity field. Note that, given the difference in the frame rate between the two cameras, the computation of the velocity field was based on a time interval equal to 25^{-1} s, corresponding to ten frames of the high-speed camera. An example of the mapping of the density field on particle trajectories is shown in Fig. 6.

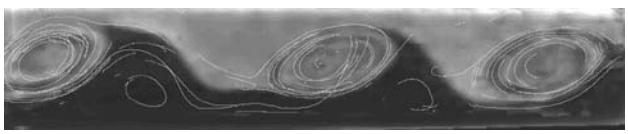

Fig. 6 Example of PTV trajectories mapped on the density field

4 Results and discussion

Dimensional analysis shows that the flow depends on three parameters (see, for example, Defina et al. 1999): the Schmidt number, the gradient Richardson number calculated at the density interface $z = 0$:

$$\mathrm{Ri}_G = \frac{g}{\rho_0}\frac{-\frac{\partial\rho}{\partial z}\big|_{z=0}}{\left(\frac{\partial u_x}{\partial z}\big|_{z=0}\right)^2}$$

and the Reynolds number,

$$\mathrm{Re} = \frac{\Delta U\, H}{\nu},$$

where ρ is the density, g is the acceleration of gravity, u_x is the longitudinal velocity component, ΔU is the velocity difference between the two layers at the onset of the instability ($t = 0$) and ρ_0 is the mean density of the fluid. The angle of tilting, θ, adopted in the experiments was sufficiently large to attain the theoretical condition $\mathrm{Ri}_G < 0.25$ for the onset of the instability (Miles 1961; Howard 1961) soon enough for the phenomenon not to be influenced by the end walls of the tank. The conditions of the experiment have been changed by varying θ and the density difference $\Delta\rho$ between the layers. The main parameters of the experiments discussed in the following are reported in Table 1, where

$$\mathrm{Ri}_B = \frac{gH\Delta\rho/\rho_0}{\Delta U^2}$$

is the bulk Richardson number. In Fig. 7, the profiles of non-dimensional density deviation, $(\langle\rho\rangle - \rho_0)/\Delta\rho$, and non-dimensional longitudinal velocity, $\langle u_x\rangle/\Delta U$, are plotted at three times during Expt #1. Here $\langle\cdot\rangle$ indicates the spatial average along the longitudinal direction computed over one KH wavelength. As the tank is tilted, the upper (lighter) layer begins to flow upwards while the lower layer flows downwards generating two asymmetric profiles. Since the tank is rotated clockwise, this means that the velocity is positive in the lower half of the tank and negative in the upper half. During this phase the flow is laminar, and no turbulent mixing between the density interface occurs. As a consequence, the density of the two

Table 1 Main parameters of the experiments

Expt #	$\Delta\rho$ (Kg/m^3)	ρ_0 (Kg/m^3)	θ (degrees)	ΔU (m/s)	Ri_B	Ri_G	Re
1	31	1036	2.9	0.197	0.166	0.096	4334
2	17	1021	3.1	0.146	0.168	0.011	3212
3	19	1022	3.8	0.152	0.173	0.096	3344
4	31	1039	2.9	0.171	0.220	0.185	3762
5	51	1009	2.3	0.240	0.189	0.090	5280

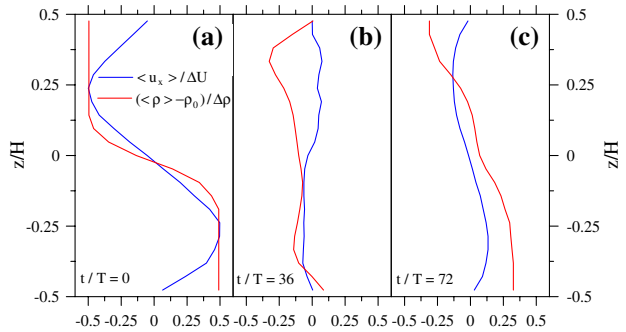

Fig. 7 Normalised velocity (*blue lines*) and density (*red lines*) profiles at (**a**) $t/T = 0$, (**b**) $t/T = 36$ and (**c**) $t/T = 72$ measured during Expt #5

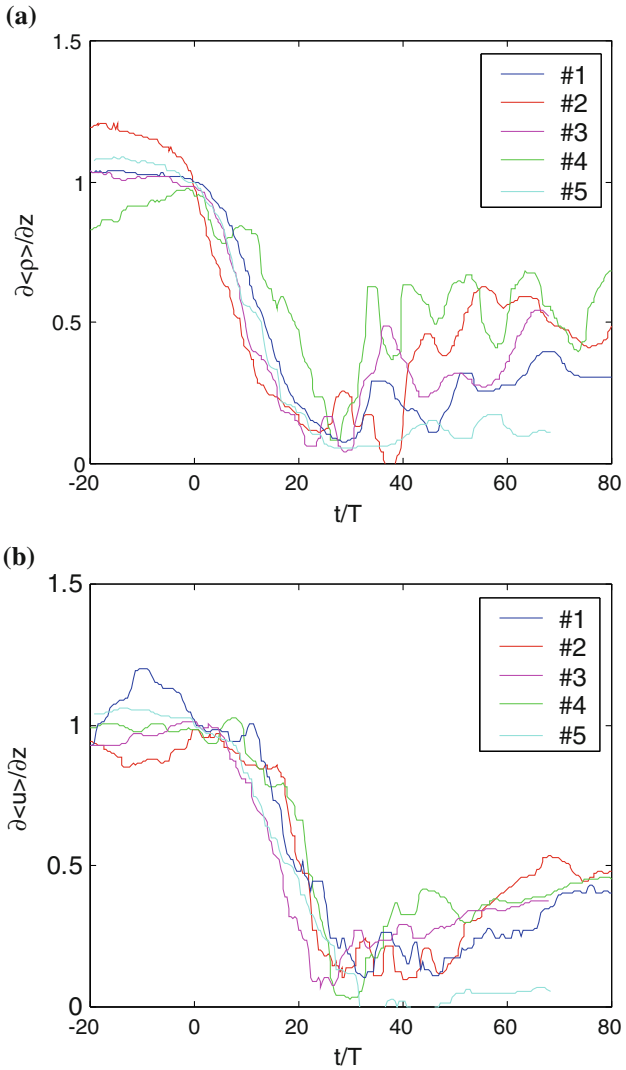

Fig. 8 Average vertical gradients of (**a**) density and (**b**) velocity at the interface ($z/H = 0.0$) as a function of the non-dimensional time, t/T, during the five experiments. Gradients are normalised by their values at $t/T = 0$

layers remains constant and the interface remains sharp. The curves in Fig. 7a represent the non-dimensional velocity (blue line) and density (red) profiles taken at $t/T = 0$, when the velocity difference is a maximum (here $T = H/\Delta U$, the advective time scale). Figure 7b describes the profiles at the non-dimensional time $t/T = 36$, after the KH waves are collapsed and the flow is strongly turbulent and characterised by an intense vertical mixing. Consequently, the longitudinal velocity is nearly zero and the density is nearly uniform over the whole depth of the central layer. However, part of the agitation generated by the KH waves does not correspond to irreversible mixing, so the flow reorganises itself again in a parallel shear flow (Fig. 7c, $t/T = 72$), characterised by a lower density gradient, in particular at the density interface, and smaller velocity differences between the two layers. It should be mentioned that the vorticity thickness, $\delta_u = \Delta U/(\partial u_x/\partial z)$, ranged from 5 to 11 mm during the initial parallel flow for all the experiments. Thus, the tank depth was always below the limit $4.4\delta_u$, indicating that the horizontal boundaries might affect the mixing properties of the flow (Haigh and Lawrence 1999).

4.1 Characteristics of the interface

The transverse gradients of velocity and density at $z = 0$ describe the intensity of the interface between the layers. The quantities have been longitudinally averaged as described above and a linear fit over the central layer of the tank has been performed. The first-order term of the linear fit is taken as the interface gradient, and then normalised by its value calculated at the appearance of the instability.

The time evolution of those gradients for the five experiments listed in Table 1 is plotted in Fig. 8. All the runs show a common general behaviour both for the density (Fig. 8a) and velocity (Fig. 8b) gradient, suggesting that, in the range of the Richardson numbers considered in the present work, the formation of the KH wave scales with the advective time T. During the phase of parallel flow preceding the appearance of the instability ($t/T < 0$), a plateau is observed (except for some low frequency fluctuations, possibly due to small oscillations of the sharp density interface). The gradients maintain their values also during the first phase of development of the waves, until they exhibit a steep decrease corresponding to the collapse of the billows with the corresponding intense turbulence. Though all the curves show a minimum at about $30T$, in the case of the velocity gradient, the plateau lasts a little longer and, consequently the decrease is steeper. After the breaking of the waves, the flow shows a partial restratification, so the velocity and density gradients increase up to about one half of their prior values. It is interesting to note that Expt #5 displays considerably smaller values of both

the velocity and density gradients after the collapse of the billow. This suggests that the presence of a more intense mixing, possibly caused by the higher Reynolds number characterising Expt #5 (see Table 1).

The thickness of the interface was evaluated by the integral density and velocity length-scales, respectively I_ρ and I_u, as proposed by Smyth and Moum (2000), and made non-dimensional by the tank height, H:

$$\begin{cases} I_\rho = \frac{1}{H}\int_{-H/2}^{H/2}\left[1-\left(2\frac{\langle\rho\rangle-\rho_0}{\Delta\rho}\right)\right]\mathrm{d}z \\ I_u = \frac{1}{H}\int_{-H/2}^{H/2}\left[1-\left(2\frac{\langle u\rangle^2}{\Delta U}\right)\right]\mathrm{d}z \end{cases}.$$

Similar to the gradients, the time evolution of the integral scales, plotted in Fig. 9, shows a common behaviour for all the runs of the experiment. The velocity integral length scale (Fig. 9a) is nearly constant, with values around 0.2 H, during the parallel flow phase. At the appearance of the instability, the scale increases until $t = 30T$, when it attains a maximum (about $0.8H$ in the majority of the runs), corresponding to the turbulent phase after the breaking of the waves. Then, during the relaminarisation of the flow, I_u decreases down to a value of $0.35H$, except for Expt #5, which gives higher values. This fact indicates that the mixing after the wave breaking was more intense, in agreement with the behaviour of the vertical gradients discussed above. The initial integral length scale of the density (Fig. 9b) is higher than the scale of the velocity ($I_\rho \cong 0.45H$). This indicates the presence of a thicker density interface. As with I_u, I_ρ is a maximum at $t \cong 30T$, after the wave breaking. In the subsequent phase, the density scale is almost constant, with a slow decrease, and reaches a value of $0.8H$ at the end of the record. Also, in this case Expt #5 shows a large increase in this scale during the developing of the KH waves, further evidence of the more intense turbulent mixing occurring in that run.

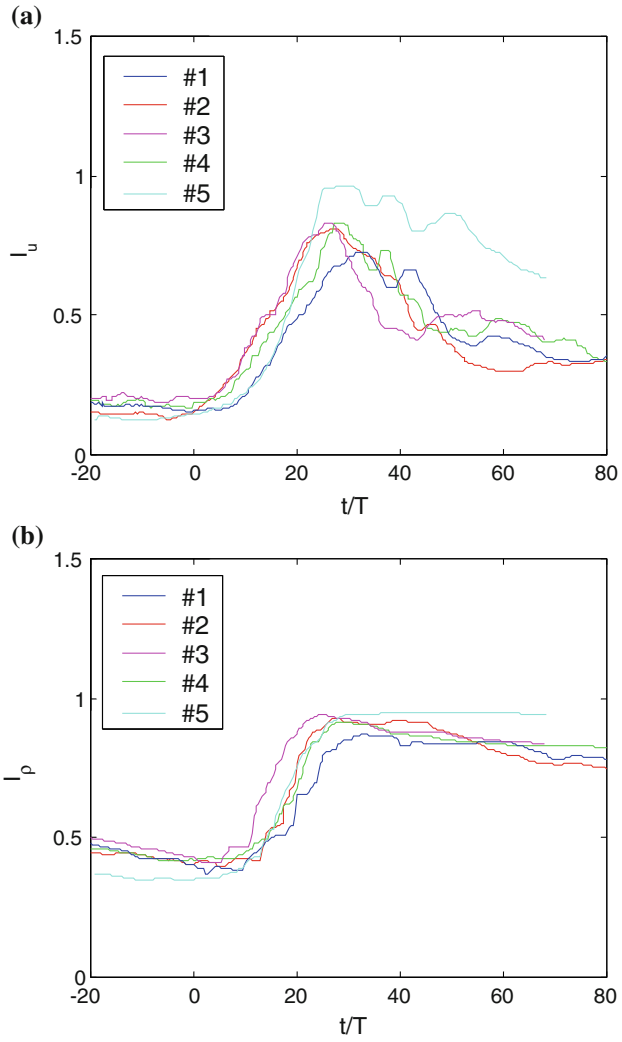

Fig. 9 Integral scale of (**a**) velocity and (**b**) density interfaces as a function of the non-dimensional time, t/T, during the five experiments. The scales are normalised by the tank height, H

4.2 Statistics

The overall evolution of the flow during the development of the KH waves is described in terms of statistics of the longitudinal and transverse velocity and of the density field. In Fig. 10, the statistics are presented for Expt #5. The quantities are made dimensionless by means of the above-defined scales. In the colour maps, the abscissa represents the non-dimensional time, t/T, and the ordinate the non-dimensional transverse position, z/H. The mean longitudinal velocity, $\langle u_x\rangle/\Delta U$, clearly exhibits (Fig. 10a) the parallel shear flow with positive velocities in the lower half of the tank and negative velocities in the upper layer observed also in Fig. 7. At $t/T \cong 0$ the sheared interface begins to grow slowly until $t/T \cong 10$. Then, the growth rate increases while the magnitude of the longitudinal velocities decrease. At $t/T \cong 27$, the velocity over the whole tank height is vanishingly small. For $t/T > 50$, the flow reorganises itself in a way similar to the one present at negative times. During that final stage the velocities are meaningfully lower.

Figure 10b and c represents, respectively, the variances of the longitudinal and transverse velocities. The longitudinal velocity variance attains a maximum during the final stage of development of the perturbations ($t/T \cong 22$), whereas the variance of the transverse component shows high values a little later, during the turbulent flow following the breaking of the waves. The strong turbulence event lasts until $t/T \cong 40$, when the restratification begins and the flow tends toward a laminar state.

The characteristics of the phenomenon are clearly recognisable also by inspection of Fig. 10d and e, where the mean and the variance of the density field are reported,

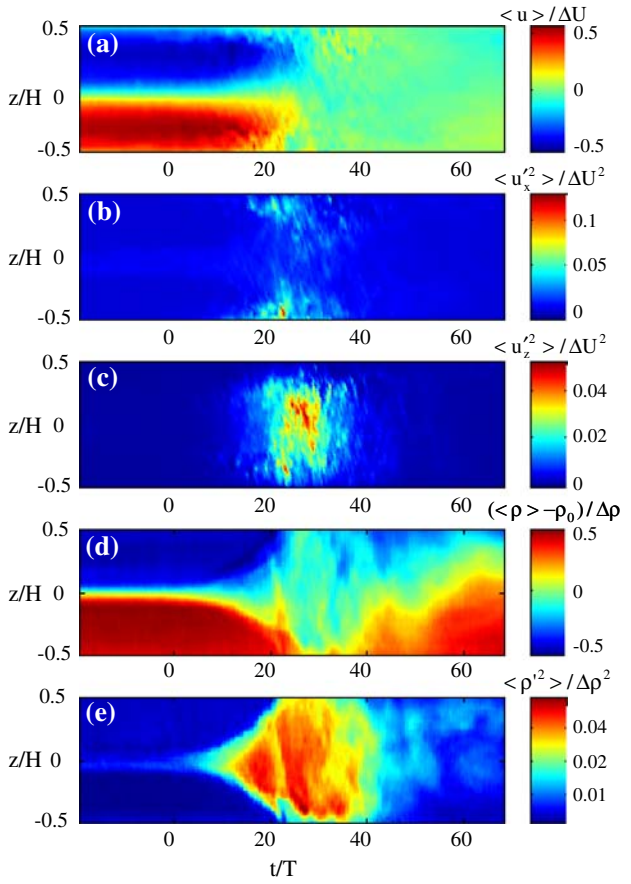

Fig. 10 Time evolution of normalised (**a**) longitudinal mean velocity, (**b**) longitudinal velocity variance, (**c**) transverse mean velocity variance, (**d**) mean density and (**e**) density variance obtained by longitudinal averaging for Expt. #5. *Abscissae* indicate non-dimensional time, *t/T*, ordinates indicate the non-dimensional transverse position, *z/H*

respectively. In particular, it is worthwhile to notice that the phase of development of the perturbation is clearly divided into two parts: in the range $0 < t < 10T$ the growth rate of the perturbations is relatively slow (about $0.05\Delta U$). That phase is characterised by the amplification of sinusoidal perturbations. At $t \cong 10T$ the waves begin to roll into the well known cat's eyes, and the rate increases to about $0.25\Delta U$, until the perturbations reach the upper and lower walls ($t \cong 27T$).

5 Conclusions

Image analysis techniques have been developed for the study of nearly parallel flows with high longitudinal velocity and transverse gradients, such the one generated at the initial stages in the tilting tank used in the present experiments. In particular, it has been shown that stretching images in the direction orthogonal to the main motion may significantly increase the effectiveness of PTV in such flows. At the same time, LIF acquisitions have been performed by a second video-camera, equipped with a narrow band filter, in order to acquire information about the density field, thus permitting the evaluation of the fundamental characteristics of the evolution and breaking of the KH wave. The density information has been described in the same reference frame as the velocity data by means of a registration procedure, based on an affine transformation, not requiring the use of any targets in the test section. The development of the parallel, stratified flow and the onset of the KH waves has been documented both in terms of the characteristics of the interface and of the statistics of the velocity and density fields. The analysis of the thickness of the density and velocity interfaces shows that, during the five experiments performed in this study, the thickness of the density interface, I_ρ, at the onset of the instability was about 2.6 times the thickness of the velocity interface, I_u. After the mixing due to the development and breaking of the wave, a counter-flowing, stratified flow appears again, because of the restratification occurring after the wave breaking. At that final stage, I_u is increased about 2 times, whereas I_ρ is increased about 1.6 times in comparison with the values before the KH appearance. Correspondingly, the intensity of the gradients is reduced down to one half of their values at the onset of the instability. Finally, the statistics of the velocity and density fields reveal that the perturbation growth occurs in two stages, with two different, but nearly constant rates. During the first stage, characterised by the amplification of sinusoidal perturbations, the growth rate is low. Successively, as the interface begins to roll into the well-known cat's eyes, the growth rate changes, attaining a value about five times higher.

References

Atsavapranee P, Gharib M (1997) Structures in stratified plane mixing layers and the effect of cross-shear. J Fluid Mech 342:53–86

Caulfield CP, Peltier WR (2000) The anatomy of the mixing transition in homogeneous and stratified free shear layers. J Fluid Mech 413:1–47

De Silva IPD, Fernando HJS, Eaton F, Hebert D (1996) Evolution of Kelvin–Helmholtz billows in nature and laboratory. Earth Planet Sci Lett 143:217–231

Defina A, Lanzoni S, Susin FM (1999) Stability of a stratified viscous shear flow in a tilted tube. Phys Fluids 11(2):344–355

Haigh SP, Lawrence GA (1999) Symmetric and nonsymmetric Hölmböe instabilities in an inviscid flow. Phys Fluids 11(6):1459–1468

Howard LN (1961) Note on a paper of John W. Miles. J Fluid Mech 10:512–512

McDougall TJ (1979) On the elimination of the refractive index variations in turbulent density stratified liquid flows. J Fluid Mech 98:83–96

Miles JW (1961) On the stability of heterogeneous shear flows. J Fluid Mech 10:496–508

Monti P, Fernando HJS, Princevac M, Chan WC, Kowalewski TA, Pardyjak ER (2002) Observations of flow and turbulence in the nocturnal boundary layer over a slope. J Atmos Sci 59(17):2513–2534

Monti P, Leuzzi G (1996) A closure to derive a three-dimensional well-mixed trajectory model for non-Gaussian, inhomogeneous turbulence. Boundary-Layer Meteorol 80:311–331

Monti P, Querzoli G, Cenedese A, Piccinini S (2007) Mixing properties of a stably stratified parallel shear layer. Phys. Fluids 19(085104):1–9

Peltier WR, Caulfield CP (2003) Mixing efficiency in stratified shear flows. Annu Rev Fluid Mech 35:135–167

Querzoli G (1996) A Lagrangian study of particle dispersion in the unstable boundary layer. Atmos Environ 30:282–291

Smyth WD, Moum JN (2000) Length scales of turbulence in stably stratified mixing layers. Phys Fluids 12(6):1327–1342

Staquet C (2000) Mixing in a stably stratified shear layer: two- and three-dimensional numerical experiments. Fluid Dyn Res 27:367–404

Thorpe SA (1968) A method of producing a shear flow in a stratified fluid. J Fluid Mech 32:693–704

Troy CD, Koseff JR (2005) The generation and quantitative visualization of breaking internal waves. Exp Fluids 38:549–562

Woods JD (1968) Wave-induced shear instability in the summer thermocline. J Fluid Mech 32:791–800

Zitová B, Flusser J (2003) Image registration methods: a survey. Image Vis Comput 21:977–1000